Development of Collective Thomson Scattering Diagnostic for Bulk and Fast Ions in the Large Helical Device*)

Masaki NISHIURA, Shin KUBO, Kenji TANAKA, Namiko TAMURA[1)], Takashi SHIMOZUMA, Takashi MUTOH, Kazuo KAWAHATA, Tetsuo WATARI, Teruo SAITO[2)], Yoshinori TATEMATSU[2)] and LHD Experiment Group

National Institute for Fusion Science, 322-6 Oroshi-cho, Toki 509-5292, Japan
[1)]*Nagoya University, Furo-cho, Chikusa-ku, Nagoya 464-8601, Japan*
[2)]*FIR FU, University of Fukui, 3-9-1 Bunkyo, Fukui 910-8507, Japan*

(Received 28 December 2010 / Accepted 1 March 2011)

The collective Thomson scattering (CTS) technique has been utilized with the backscattering configuration to diagnose the bulk and fast ions in the Large Helical Device (LHD). The spectrogram of the scattered radiation presents the transient phenomena related to fast ion slowing down in auxiliary neutral beam heated plasmas. This is obtained by the broad band receiver resolving with 32 channels, while the probing beam from 77 GHz gyrotron is modulated with 50 Hz and is injected into plasmas. In the same shot, especially in low temperature plasma (T_e, T_i < 1 keV), a wave excitation is also observed in a narrow frequency band. The peaks in the CTS spectrum exist between 0.5 and 1.0 GHz and are observed in both frequency sides asymmetry. For the forthcoming experiments, the feasibility of CTS diagnostics at a new port location is assessed to extend the diagnostic capability for measuring the ion velocity components. Expected spectra for scattered radiation are the same signal level as the present location from a numerical calculation.

Keywords: collective Thomson scattering, ion temperature, fast ion, velocity distribution function, fusion plasmas, lower hybrid wave

DOI: 10.1585/pfr.6.2402068

1. Introduction

Collective Thomson scattering system has been developed to measure the velocity distribution function in JET, TEXTOR, ASDEX-UG, and has been designed for ITER [1–3] in fusion plasma diagnostics. The high power gyrotron with the frequencies of 140, 110, 105, and 60 GHz and the power of a few hundred kW ∼ MW is utilized as a probing beam for each device. The scattered radiation is resolved at a receiver to obtain the scattered spectra, which is analyzed by the scattering theory based on the electromagnetic fluctuation.

For the feasibility studies in the Large Helical Device (LHD), the signal level of scattered radiation and the frequency shift from the incident wave have been estimated by the scattering theory with electrostatic term [4], based on the scattering form factor introduced by Vahala *et al*. [5] and Hughes *et al*. [6]. The heterodyne receiver system has been developed. However, their detected fluctuations still needs the treatment of geometrical form factor attributed to the plasma dispersion relation for the incident and scattered electromagnetic waves. The geometrical form factor by Hughes *et al*. [7] is included in our CTS spectrum calculations.

In the last campaign of 2008, we have installed the CTS receiver system, and then have obtained the initial result of the scattered spectra measured by CTS diagnostic [8, 9]. Then the probe beam is provided by the 77 GHz gyrotron (The nominal frequency is 76.95 GHz.) with ∼ 500 kW. The scattered radiation is resolved into 8 channels at the receiver system. For more accurate velocity distribution function measurements, the number of channels is increased from 8 to 32 channels.

The LHD has unique neutral beam (NB) heating systems, which provide the perpendicular neutral beams with the energy of 40 keV and the parallel neutral beams with that of 180 keV. These energetic particle sources become a good confirmation in view of theoretical and experimental aspects for CTS diagnostics as well as energetic particle physics for burning plasma experiments. The fast ions have anisotropic distribution just after the neutral beam injection, and are thermalized due to the coulomb collisions with other charged particles in plasmas. The expected scattered spectra are calculated for the backscattering configuration, because the available antennas are restricted in a driving range for probing and receiving beams.

2. CTS Receiver System with 32 Channels

The CTS receiver system resolves into the 32 channels

author's e-mail: nishiura@nifs.ac.jp

*) This article is based on the presentation at the 20th International Toki Conference (ITC20).

to reconstruct a scattered radiation. The detail of the receiver system is denoted in Ref. [10]. The heterodyne detection is utilized for the scattered radiation from the 77 GHz gyrotron beam. The scattered radiation is separated into the receiver channels, which have two kinds of band widths of 100 MHz for bulk ions and 200 MHz for fast ions in the frequency between ± 2.5 GHz. The detection efficiency for each channel of the CTS receiver system is obtained from the radiation of Liquid N_2. The synthetic CTS spectrum is reconstructed by convoluting the original CTS spectrum with the detection efficiency and the characteristics on the band pass filters and the notch filter, as is shown in Fig. 1. Here the original CTS spectrum is calculated numerically based on the theory of scattered radiation in Vahala *et al*. [5] and Hughes *et al*. [6]. The characteristics of each band pass filter for the filter bank and the notch filter for the rejection of an intense stray radiation of 76.95 GHz gyrotron beam are measured by a network analyzer. The probing and receiving beams is injected from the 9.5-U port of the LHD, which is the vertically elongated elliptical cross section in Fig. 2. The wave vector $\boldsymbol{k}^{\delta} = \boldsymbol{k}^{s} - \boldsymbol{k}^{i}$, and the frequency shift $f = f_s - f_i$ (or $\omega = \omega_s - \omega_i$) are due to the wave -plasma interaction, where $\boldsymbol{k}^{s}$ and $\boldsymbol{k}^{i}$ are the scattered and the incident wave vectors, respectively. The scattering volume, where two beams overlap, is located at $(R, T, Z) = (3.6, 0, 0)$ in meter. The probing beam power is set to 100 kW for the calculation. From Fig. 1, we found that the synthetic CTS spectrum in closed symbols is in good agreement with the original one in solid line. Therefore the receiver system is capable of the reconstruction in CTS spectrum.

The theoretical CTS spectrum is composed of electrons, ions, and fast hydrogen ions. The dominant CTS signal for the fast hydrogen ions with the slowing down distribution is located near the frequency of ± 1 GHz. The fast ion radiation level must also overcome the background electron cyclotron emission.

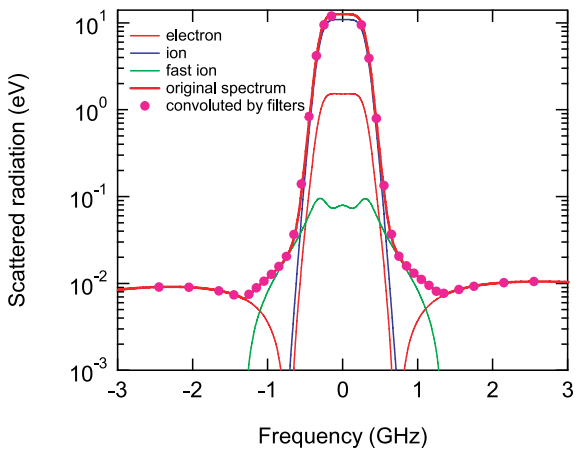

Fig. 1 Synthetic CTS spectrum at diode detectors after the convolution of the system response function. The original CTS spectrum is calculated numerically in the case of $T_e = T_i = 1$ keV, $T_{fast} = 40$ keV with slowing down distribution, $n_e = 1 \times 10^{19}$ m^{-3}, $n_i = 0.99 \times 10^{19}$ m^{-3}, and $n_{fast} = 0.01 \times 10^{19}$ m^{-3} at $R_{ax} = 3.6$ m and $B_t = 2.4$ T.

3. Time Evolution of Bulk and Fast Ions by CTS Spectrum

Understanding of the relaxation processes of the fast ions and their transport are important for self-burning plasmas. As a test particle of fast ions, a neutral hydrogen beam (NB) with the energy of about 40 keV is injected perpendicular to the magnetic field of the LHD. The geometry of the CTS probing and receiving beams is shown in Fig. 2. The schematic shows the poloidal projection of the LHD. Since the angle between $\boldsymbol{k}^{\delta}$ and the magnetic field at the scattering volume $(R, T, Z) = (3.6, 0, 0)$ is 79.6 degrees, the CTS diagnostic is sensitive relatively to the perpendicular velocity component rather than the parallel one with respect to the magnetic field.

Figure 3 (d) shows the spectrogram of the scattered radiation by CTS during the neutral beam injection in a typical LHD plasma shot. The measured signal is averaged over 1 ms. The probing beam power of 640 kW is modulated at the frequency of 50 Hz, and then the scattered radiation is obtained by subtracting the background radiation just after the off timing of the rectangular wave form from the measured signal at the on timing. Plasma parameters are also plotted in the figures from (e) to (g). The intensity of scattered radiation is normalized by the electron density n_e, which is measured by the incoherent Thomson scattering, in order to compare between CTS spectra. The

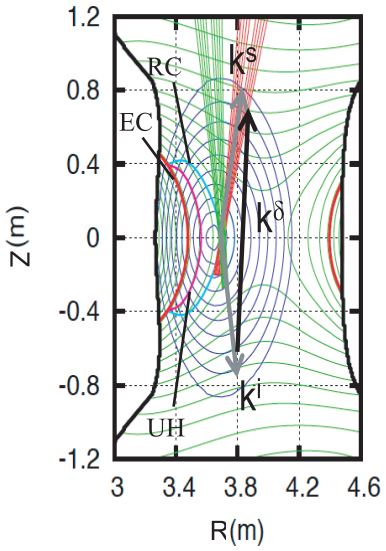

Fig. 2 Scattering geometry for probing and receiving beams in LHD poloidal cross section in the case of $R_{ax} = 3.6$ m, $B_t = 2.4$ T. The magnetic flux surfaces are plotted in a blue line. The electron cyclotron resonance layer(EC) and the upper hybrid resonance layer(UH), the R-cut off layer(RC) are indicated.

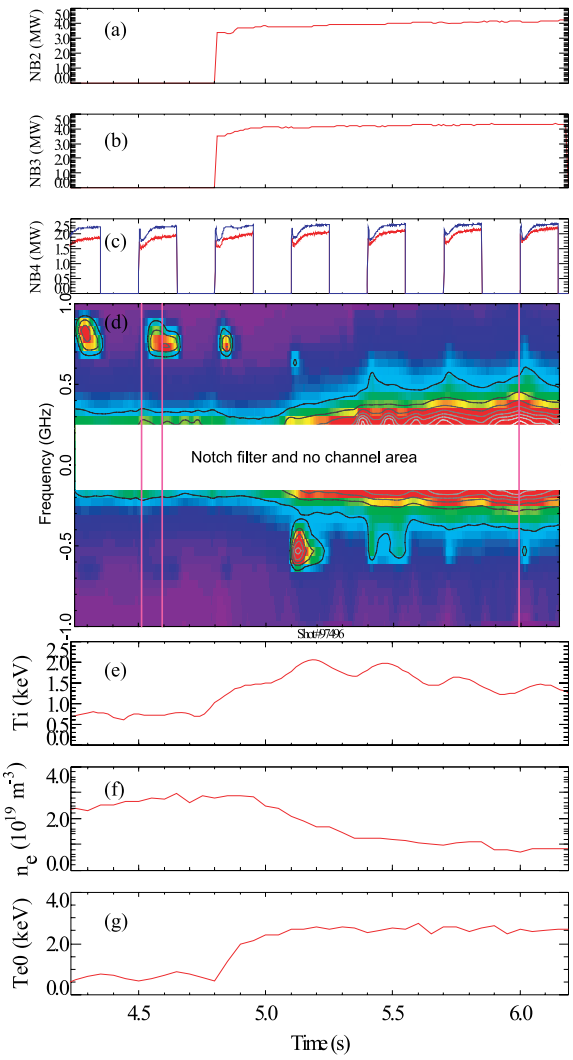

Fig. 3 Time evolution of CTS spectrum for LHD#97496. The injection powers of (a) Co-NB2, (b) Ctr-NB3, (c) Perp.-NB4. (d) Spectrogram of scattered radiation measured by CTS. (e) Ion temperature T_i from Ar line spectroscopy. (f) Electron density and (g) Electron temperature are measured by the incoherent Thomson scattering at the plasma center.

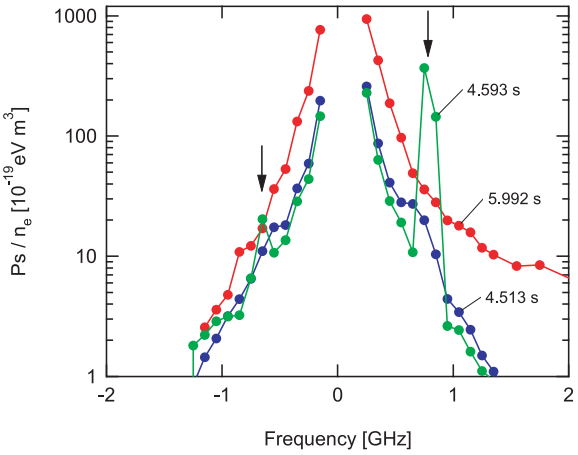

Fig. 4 The CTS spectra at t = 4.513, 4.593 and 5.992 s at LHD#97496. The scattered radiation is normalized by the electron density. The excited wave is observed at t = 4.593 s on CTS spectrum. The arrows indicate the frequencies of the excited wave.

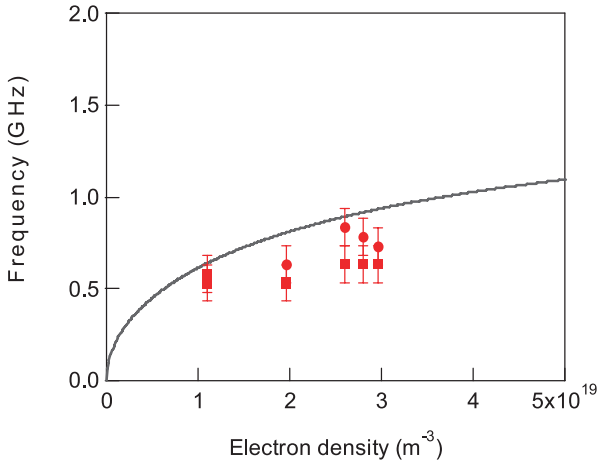

Fig. 5 Frequencies of excited wave (closed symbols) and the lower hybrid wave (solid curve) are plotted as a function of the electron density.

co-NB3, the counter-NB2, and the perpendicular NB4 are injected with each power of 4 MW for the plasma production and sustainment. At the time frame from 4.2 to 4.8 s during only NB4 injection, the CTS spectrum for the bulk ions ($< \pm$ 0.4 GHz) is narrower than that at the time frame of 5.0 s and later. The expansion of the CTS spectrum is reasonably explained by the increase of T_i in Fig. 3 (e).

The slowing down process of fast ions is observed at the frequencies of +0.5 GHz and −0.5 GHz during NB4 injection. The asymmetric shape of CTS spectra might be explained by $\boldsymbol{k}^{\delta}$ with the angle of 10.4 degrees deviated away from the normal axis to the magnetic field.

The strong peak is also observed at the frequency around 0.5 to 1.0 GHz in positive and negative frequencies. The detail CTS spectra at t = 4.513 s (just after injecting NB4 beam), 4.593 s (during injecting NB4 beams) and 5.992 s (before injecting NB4 beams) are plotted in Fig. 4. The distinctive peaks at t = 4.593 s appear at low T_e and T_i (less than 1 keV) and only in the existence of fast ions with perpendicular velocity produced by NB4. However, as T_e and T_i increase gradually with the decrease of n_e and fast ions with parallel velocity are produced by co- and counter NBs, the peak frequencies shift to downward and merge to the bulk ion region. This phenomenon is considered not to be a change of the distribution function of fast ions related to 40 keV NB, but to be an excitation of a NB driven turbulence such as lower hybrid waves, which are pointed out at W7-AS [11]. The frequencies of perpendicular fast ion driven waves and theoretical lower hybrid waves are plotted as a function of the electron density in Fig. 5. The lower hybrid wave is calculated by the relation as the cold magnetized plasma approximation [11],

$\omega_{LH}^2 = \omega_{pi}^2/(1+\omega_{pe}^2/\omega_{ce}^2)$. Here, ω_{pi}, ω_{pe}, and ω_{ce} are the ion plasma frequency, the electron plasma frequency, and the electron cyclotron frequency, respectively. From the comparison, the measured frequencies of the perpendicular fast ion driven wave are slightly lower than those of the lower hybrid wave. The careful analysis will be carried out for the identification of perpendicular fast ion driven waves.

4. Feasibility of CTS Diagnostic at New Location

To extend the diagnostic capability, the CTS signal levels are estimated numerically at some locations, as shown in Fig. 6. When we use the probing and receiving beams at new locations (a) and (b), the CTS diagnostic can cover the wider plasma areas (the normalized plasma radius, $r/a < \sim 1$) at new locations than that ($r/a < \sim 0.5$) at the present location (c), because of the mechanical design for electron cyclotron heating.

The scattered power P_s is inferred from the electrostatic fluctuation estimated using the following relation [6],

$$P_s = P_i \Gamma r_e^2 n_e d\omega \frac{\lambda_{s0}^2}{2\pi (2r_R \sin\theta_r)} S(k^\delta, \omega), \qquad (1)$$

where P_i is the incident beam power, r_e is the classical electron radius, n_e is the electron density, $d\omega$ is band width, r_R is the beam radius, λ_{s0} is the wavelength of scattered radiation. The geometrical factor Γ in the above equation is assumed to be one in the previous paper, while the dielectric properties are carefully treated in this paper with the same manner of Ref. [6]. The scattering volume is precisely calculated by Kubo *et al.* [8], taking into account the power density effect. The form factor $S(k^\delta, \omega)$ is calculated by using the plasma dispersion function. The location in Fig. 6 (c) is the present configuration with the angle of $\angle(\boldsymbol{k}^\delta, \boldsymbol{B}) = 100.5°$. This configuration can measure nearly perpendicular velocity components. For the more flexible diagnostics, the case (b) with the new diagnostic location is calculated. Two antenna systems for electron cyclotron heating (ECH) have been already installed into the port, and one of them is possible for the CTS diagnostic. The signal level of the scattered radiation is estimated by using the Eq. (1). The input parameters, the geometrical parameters and the wave vectors are summarized in Tables 1 and 2, respectively. Figure 7 shows the comparison of calculated CTS spectra between the present location (c) and the

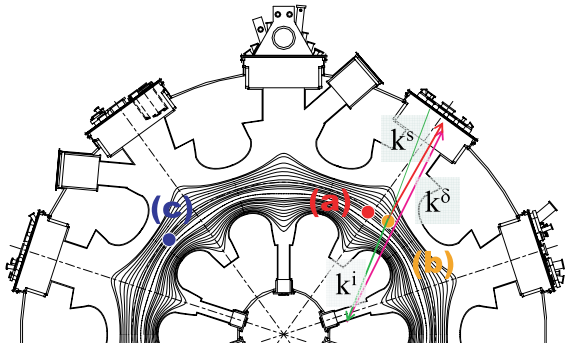

Fig. 6 Top view of LHD and magnetic field at the mid plane. Locations (a) and (b) at the new port for CTS diagnostics. Location (c) is used for the present measurement.

Table 1 Common input parameters for the calculation of Eq. (1).

R_{ax}	3.6 m
B_t	2.4 T (counter clockwise)
r_R	0.015 m
f_g	77 GHz
P_i	100 kW

n_e	1×10^{19} m^{-3}	T_e	1 keV
n_i	0.99×10^{19} m^{-3}	T_i	1 keV
n_{fast}	0.01×10^{19} m^{-3}	T_{fast}*	180 keV

*T_{fast} is the maximum energy with slowing down distribution.

Table 2 Geometrical parameters and wave vectors for CTS spectrum calculations in the LHD.

		Location (a) (3.6, 0, 0) θ_{tor} = 54 deg.	Location (b) (3.6, -0.79, 0) θ_{tor} = 54 deg.	Present (c) (3.6, 0, 0) θ_{tor} = 144 deg.
θ_r	[deg.]	170.8	171.0	165.2
ϕ_i	[deg.]	95.1	108.5	76.2
$\lvert\boldsymbol{k}^i\rvert$ in vac.	[m^{-1}]	1613.8	1613.8	1613.8
$\lvert\boldsymbol{k}^i\rvert$	[m^{-1}]	1500.9	1509.5	1505.6
ϕ_s	[deg.]	95.6	81.6	96.9
$\lvert\boldsymbol{k}^s\rvert$	[m^{-1}]	1388.0	1389.2	1388.5
ϕ_δ	[deg.]	90.0	76.3	100.5
$\lvert\boldsymbol{k}^\delta\rvert$	[m^{-1}]	2876.3	2887.5	2869.2
k_{para}	[m^{-1}]	-1.29	682.3	-525.8
k_{perp}	[m^{-1}]	2876.3	2805.7	2820.7

θ_r is the angle between incident and received ray directions.
ϕ_i is the angle between incident wave vector and magnetic field.
ϕ_s is the angle between scattered wave vector and magnetic field.
ϕ_δ is the angle between $\boldsymbol{k}^\delta$ and magnetic field.

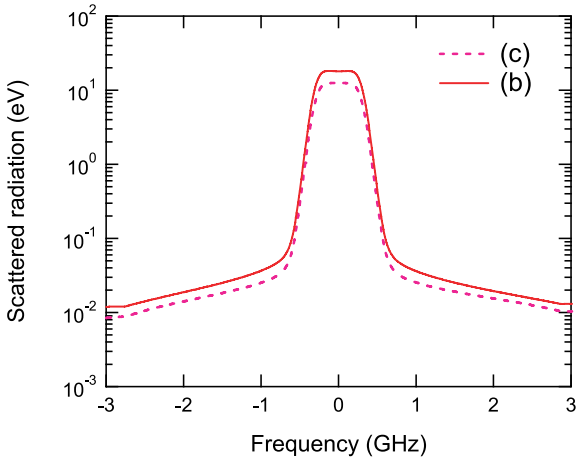

Fig. 7 Calculated CTS spectra at the new location (b) and the present location (c) in the LHD. Parameters required are summarized in Tables 1 and 2.

new location (b). The expected signal at the new location (b) is the same level as the present location (c). If the background radiation is supposed to be a same level as the location (c), we could maintain the signal to noise ratio for the CTS diagnostic enough.

Near perpendicular location (a), the CTS spectrum includes another excited wave such as an ion Bernstein wave [12]. This will be used as an option to measure the fueling ratio of hydrogen to deuterium ions. To suppress the wave excitations, the CTS spectra are surveyed numerically, and it is found that the angle of $\angle(\boldsymbol{k}^{\delta}, \boldsymbol{B}) \leq 80^{\circ}$ or $\geq 100^{\circ}$ should be selected by changing a diagnostic location toroidally and vertically with keeping a same normalized minor radius.

5. Summary

The CTS diagnostic has been carried out in NB heated LHD plasmas. The time evolution of scattered radiation is successfully obtained by using the CTS receiver system. When the perpendicular fast ions exist, the excited wave is observed in CTS spectra. These frequencies are close to those of the lower hybrid wave. However the detail analysis and experiments are still necessary for the identification of excited waves.

To extend the diagnostic plasma areas, the feasibility of CTS diagnostics at a new port location is assessed. Expected spectra for scattered radiation are the same signal level as the present location from the numerical calculations. The location of $\angle(\boldsymbol{k}^{\delta}, \boldsymbol{B}) \sim 90^{\circ}$ would be an option of measuring the fueling ratio.

Acknowledgement

We would like to thank to the CTS group at Risö DTU for the collaborative work. This work is supported by the National Institute for Fusion Science under NIFS09ULRR526, NIFS10ULRR004, and Grant-in-Aid for Scientific Research (B)#21360455.

[1] H. Bindslev, J.A. Hoekzema, J. Egedal, J.A. Fessey, T.P. Hughes and J.S. Machuzak, Phys. Rev. Lett. **83**, 3206 (1999).
[2] S.B. Korsholm, H. Bindslev, F. Meo, F. Leipold, P.K. Michelsen, S. Michelsen, P. Woskov, E. Westerhof, FOM ECRH team, J.W. Oosterbeek, J. Hoekzema, F. Leuterer, D. Wagner and ASDEX Upgrade ECRH team, Rev. Sci. Instrum. **77**, 10E514 (2006).
[3] F. Meo, H. Bindslev, S.B. Korsholm, E.L. Tsakadze, C.I. Walker, P. Woskov and G. Vayakis, Rev. Sci. Instrum. **75**, 3585 (2004).
[4] M. Nishiura, K. Tanaka, S. Kubo, T. Saito, Y. Tatematsu, T. Notake, K. Kawahata, T. Shimozuma and T. Mutoh, Rev. Sci. Instrum. **79**, 10E731 (2008).
[5] L. Vahala, G. Vahala and D.J. Sigmar, Nucl. Fusion **26**, 51 (1986).
[6] T.P. Hughes and S.R.P. Smith, Nucl. Fusion **28**, 1451 (1988).
[7] T.P. Hughes and S.R.P. Smith, J. Plasma Phys. **42**, 215 (1989).
[8] S. Kubo, M. Nishiura, K. Tanaka, T. Shimozuma, Y. Tatematsu, T. Notake, T. Saito, Y. Yoshimura, H. Igami and N. Tamura, Plasma Fusion Res. **5**, S1038 (2010).
[9] M. Nishiura, S. Kubo, K. Tanaka, N. Tamura, T. Shimozuma, T. Mutoh, K. Kawahata, T. Watari, T. Saito, Y. Tatematsu, T. Notake and LHD experiment group, J. Phys. conference series **227**, 012014 (2010).
[10] S. Kubo, M. Nishiura, K. Tanaka, T. Shimozuma, Y. Yoshimura, H. Igami, H. Takahashi, T. Mutoh, N. Tamura, Y. Tatematsu, T. Saito, T. Notake, S.B. Korsholm, F. Meo, S.K. Nielsen, M. Salewski and M. Stejner, Rev. Sci. Instrum. **81**, 10D535 (2010).
[11] E.V. Suvorov, V. Erckmann, E. Holzhauer, W.Y.A. Dryagin, S.E. Filchenkov, A.A. Fraiman, T. Geist, M. Kick, L.M. Kukin, A.V. Kostrov, L.V. Lubyako, A.M. Shtanyuk, N.K. Skalyga, O.B. Smolyakova, W VII-AS Team and NBI Team, Plasma Phys. Control. Fusion **37**, 1207 (1995).
[12] M. Stejner, S.K. Nielsen, S.B. Korsholm, M. Salewski, H. Bindslev, V. Furtula, F. Leipold, F. Meo, P.K. Michelsen, D. Moseev, A. Bürger, M. Kantor and M. de Baar, Rev. Sci. Instrum. **81**, 10D515 (2010).